Journal of Industrial and Engineering Chemistry 19 (2013) 806–812

Contents lists available at SciVerse ScienceDirect

Journal of Industrial and Engineering Chemistry

journal homepage: www.elsevier.com/locate/jiec

Conversion of syngas to C_2^+ oxygenates over Rh-based/SiO_2 catalyst: The promoting effect of Fe

Jun Yu, Dongsen Mao *, Lupeng Han, Qiangsheng Guo, Guanzhong Lu

Research Institute of Applied Catalysis, School of Chemical and Environmental Engineering, Shanghai Institute of Technology, Shanghai 201418, China

ARTICLE INFO

Article history:
Received 23 June 2012
Accepted 20 October 2012
Available online 29 October 2012

Keywords:
Fe promoter
Rh–Mn–Li/SiO_2
CO hydrogenation
C_2^+ oxygenates

ABSTRACT

The effect of Fe promoter on the catalytic properties of Rh–Mn–Li/SiO_2 catalyst for CO hydrogenation was investigated. The catalysts were comprehensively characterized by means of X-ray diffraction (XRD), N_2 adsorption–desorption, temperature programmed reduction (TPR), temperature programmed desorption (TPD), temperature programmed surface reaction (TPSR), and diffuse reflectance infrared Fourier transform spectroscopy (DRIFTS). Activity testing results showed that low loading of Fe ($\leq$0.1 wt%) improved the reactivity and yield of C_2^+ oxygenates; however, the opposite effect appeared at the high values of Fe (>0.1 wt%). Characterization results suggested that the addition of Fe strengthened the Rh–Mn interaction and increased the desorption/transformation rate of adsorbed CO, which could be responsible for the increase of CO conversion. But on the other hand, the existence of Fe might deposit over the Rh surface, and decreased the number of active sites, resulting in the decrease of CO conversion when the Fe amount was excessive. The selectivity to C_2^+ oxygenates varied inversely with the reducibility of Rh oxide species. Moreover, it is proposed that the transformation of dicarbonyl $Rh^+(CO)_2$ into H–Rh–CO is favorable for the formation of C_2^+ oxygenates, and the hydrogenation ability of Fe can increase the hydrogenation of acetaldehyde to ethanol.

1. Introduction

C_2 oxygenates such as ethanol, acetaldehyde and acetic acid are important chemicals, and developing new types of catalysts to synthesize these oxygenated compounds from synthesis gas (syngas) is very meaningful for societal sustainable development because of the desire to decrease the global dependence on petroleum [1,2]. So far, silica (SiO_2) supported rhodium catalysts (Rh/SiO_2) have been extensively studied because they exhibit an excellent catalytic performance for C_2 oxygenates synthesis from syngas [3–5]. However, the CO conversion and selectivity of C_2 oxygenates over Rh-based/SiO_2 catalysts are still not enough for practical use. In order to further improve the catalytic properties of Rh-based/SiO_2 catalysts, the modification of additives and SiO_2 support has been investigated continuously in the past decades [6–15].

In our previous work, we have found that the Rh–Mn–Li catalyst supported on a novel SiO_2(SM) prepared by the Stöber method, exhibited higher activity and C_2 oxygenates selectivity compared with that on a commercial SiO_2 [16]. The excellent performance of the Rh–Mn–Li/SiO_2(SM) catalyst can be attributed to the special interaction between Rh particles and weakly H-bonded hydroxyls over SiO_2(SM), which promotes the CO dissociation and CO insertion. On the other band, Fe as a promoter has been investigated extensively, because of its interesting promoting effects on the catalytic performance of Rh-based catalysts for CO hydrogenation, and a number of explanations have been made to interpret the role of Fe. According to Yin et al. [12], it is concluded that the promoting effect of Fe is mainly due to its high dispersion and close contact with Rh and Mn. Guglielminotti et al. [11] proposed that the Rh sites available for CO and H_2 chemisorptions decreased upon the addition of Fe, but doubly bonded CO (Rh–CO–Fe) increased. Thus the formation of oxygenate products was favored. Moreover, some reports also suggested that sites at the Rh/Fe interface are likely to be of importance, while hydrogen spillover from Rh to Fe oxides is thought to be necessary for rapid hydrogenation of acetaldehyde [17–19]. Nevertheless, to our best knowledge, no agreement regarding the promoting mechanism of Fe has been arrived yet. Based on the above results, we considered that the Fe promoter can be tried to further enhance the catalytic performance of Rh–Mn–Li catalyst supported on the SiO_2 prepared by the Stöber method, and the further understanding of the role of Fe is also meaningful for the catalyst design.

* Corresponding author at: Shanghai Institute of Technology, Shanghai 201418, China. Tel.: +86 21 6087 7221; fax: +86 21 6087 7231.
E-mail address: dsmao@sit.edu.cn (D. Mao).

1226-086X/$ – see front matter © 2012 The Korean Society of Industrial and Engineering Chemistry. Published by Elsevier B.V. All rights reserved.
http://dx.doi.org/10.1016/j.jiec.2012.10.021

In the present study, the catalytic activities of various amounts of Fe promoted Rh–Mn–Li/SiO_2 catalysts for CO hydrogenation were compared. Furthermore, the new insights into the effect of Fe on Rh–Mn–Li/SiO_2 for CO hydrogenation were demonstrated by diffuse reflectance infrared Fourier transform spectroscopy (DRIFTS), temperature programmed reduction with H_2 (H_2-TPR), temperature programmed desorption of CO (CO-TPD), and temperature programmed surface reaction (TPSR).

2. Experimental

2.1. Catalyst preparation

SiO_2 was prepared by the Stöber method as reported in Ref. [16]. In a typical synthesis, the solution A was prepared by mixing 21 mL tetraethylorthosilicate (TEOS) (99.5%, SCRC) with 50 mL anhydrous ethanol (99.7%, SCRC); the solution B was a mixture of 76 mL $NH_3{\cdot}H_2O$ (26 vol%, SCRC) and 200 mL anhydrous ethanol. Secondly, the solution A was added slowly into the solution B in a flask under rapid stirring at 25 °C and reacted for 4 h. The white solid product was recovered by centrifugation (7000 rpm), washed with absolute ethanol for three times and then dried at 90 °C. Before used, it was calcined in static air at 350 °C for 4 h.

$RhCl_3$ hydrate (Rh ~ 36 wt%, Fluka), $Mn(NO_3)_2{\cdot}6H_2O$ (99.99%, SCRC), $Fe(NO_3)_3{\cdot}6H_2O$ (99.99%, SCRC), and Li_2CO_3 (99.5%, SCRC) were used in catalyst preparations. Catalysts were prepared by co-impregnation to incipient wetness of SiO_2 (1.0 g) with an aqueous solution of $RhCl_3$ hydrate and aqueous solutions of precursors of the promoters, followed by drying at 90 °C for 4 h, and then at 120 °C overnight before being calcined in air at 350 °C for 4 h. The weight percent of Rh, Mn, and Li is 1.5%, 1.5%, and 0.07%, respectively, and that of Fe is listed in related tables and figures. Elemental analysis by ICP-OES revealed good agreement between the expected and experimental values.

2.2. CO hydrogenation

CO hydrogenation was performed in a fixed-bed microreactor with length ~350 mm and internal diameter ~5 mm. The catalyst (0.3 g) diluted with inert α-alumina (1.2 g) was loaded between quartz wool and axially centered in the reactor tube, with the temperature monitored by a thermocouple close to the catalyst bed. Prior to reaction, the catalyst was heated to 400 °C (heating rate ~ 3 °C/min) and reduced with H_2/N_2 (molar ratio of H_2/N_2 = 1/9, total flow rate = 50 mL/min) for 2 h at atmospheric pressure. Then, the reactor was cooled to 260 °C and the reaction started at a space velocity (SV) of 10,000 mL/(g h) and pressure of 3 MPa. The feed gas contained 60% H_2, 30% CO and 10% N_2. The catalytic properties were tested at different temperatures (260 °C, 280 °C, 300 °C, and 320 °C) after the steady state reached, and the reactor temperature was increased at a heating ramp of 5 °C/min. All post-reactor lines and valves were heated to 150 °C to prevent product condensation. The products were analyzed on-line (Agilent GC 6820) using a HP-PLOT/Q column (30 m, 0.32 mm ID) with a flame ionization detector (FID) and a TDX-01 column with a thermal conductivity detector (TCD). The CO conversion was calculated based on the fraction of CO that formed carbon-containing products according to: %conversion = $(\sum n_i M_i / M_{CO}) \cdot 100$, where n_i is the number of carbon atoms in product i, M_i is the percentage of product i detected, and M_{CO} is the percentage of CO in the syngas feed. The selectivity of a certain product was calculated based on carbon efficiency using the formula $n_i C_i / \sum n_i C_i$, where n_i and C_i are the carbon number and molar concentration of the ith product, respectively.

2.3. Catalyst characterization

XRD analysis of samples was performed using a PANalytical X'Pert diffractometer operating with Ni β-filtered Cu Kα (λ = 0.15418 nm) radiation at 40 kV and 40 mA. Two theta angles ranged from 20 to 80° with a speed of 6° per minute. Transmission electron microscopy (TEM) images were obtained by JEM-2100 operated at 200 kV. BET specific surface areas of the samples were determined by N_2 adsorption isotherms, using a Micromeritics ASAP 2020 M+C adsorption apparatus. Prior to N_2 adsorption, the catalyst samples were degassed under a vacuum of 0.1 Pa for 10 h at 200 °C.

CO adsorption was studied using a Nicolet 6700 FT-IR spectrometer equipped with a DRIFT cell with CaF_2 windows. The sample in the cell was pretreated in H_2/N_2 (molar ratio of H_2/N_2 = 1/9) at 400 °C for 2 h, and then the temperature was dropped to room temperature. After the cell was outgassed in vacuum to $<10^{-3}$ Pa, the background was recorded. After CO was introduced for 80 min ($p_{co} = 8.0 \times 10^3$ Pa), the IR spectrum of CO adsorbed on the catalyst was recorded. Then the mixture of H_2/N_2 was introduced again, and the IR spectrum of CO adsorbed was recorded as a function of time. The concentration of CO was higher than 99.97%, and it was pretreated by dehydration and deoxygenization before being used. The spectral resolution was 4 cm^{-1} and the number of scans was 64.

CO-TPD or H_2-TPR was carried out in a quartz microreactor. For TPD measurements, the catalyst (0.1 g) was reduced in situ for 2 h at 400 °C in H_2/N_2 (molar ratio of H_2/N_2 = 1/9), followed by flushing with a He flow for 30 min at the same temperature before cooling down to room temperature. The next step was CO adsorption at room temperature for 30 min, and then the gas was swept again with He for 3 h. Subsequently, the sample was heated in a flowing He stream (50 mL/min) up to 750 °C at a rate of 10 °C/min with a quadruple mass spectrometer (QMS, Balzers OmniStar 200) as the detector to monitor the desorbed species. For TPR measurements, 0.05 g of the sample was first pretreated at 350 °C in O_2/N_2 (molar ratio of O_2/N_2 = 1/4) for 1 h prior to a TPR measurement. During the TPR experiment, H_2/N_2 (molar ratio of H_2/N_2 = 1/9) was used at 50 mL/min and the temperature was ramped from room temperature to 500 °C at 10 °C/min while the effluent gas was analyzed with a TCD.

The TPSR experiments were carried out as follows: after the catalyst was reduced at 400 °C in H_2/N_2 (molar ratio of H_2/N_2 = 1/9) for 2 h, it was cooled down to room temperature and CO was introduced for adsorption for 0.5 h; afterwards, the H_2/N_2 mixture was swept again, and the temperature was increased at the rate of 10 °C/min with a QMS as the detector to monitor the signals of CH_4 (m/z = 15), CO (m/z = 28) and CO_2 (m/z = 44).

3. Results and discussion

3.1. Catalyst characterization

Firstly, the catalysts were characterized by XRD, TEM and N_2 adsorption–desorption. XRD patterns (not shown) of the support and the corresponding catalysts showed no crystalline phases, indicating that the SiO_2 is XRD-amorphous and the metal particles are highly dispersed on the SiO_2 support due to their small contents. The TEM micrographs of the catalysts are shown in Fig. 1. It can be seen that the particle sizes of the metals are very small, and mainly distribute in 1–5 nm. The results suggest that the particle distribution on the surface of catalysts is highly dispersed and similar, which is consistent with that obtained by XRD. Therefore, a particle size effect can be excluded as explaining the effects of Fe promoter on the activity and selectivity of the Rh–Mn–Li/SiO_2 catalyst. On the other hand, similar BET surface areas (~15 m^2/g) were obtained on all the catalysts.

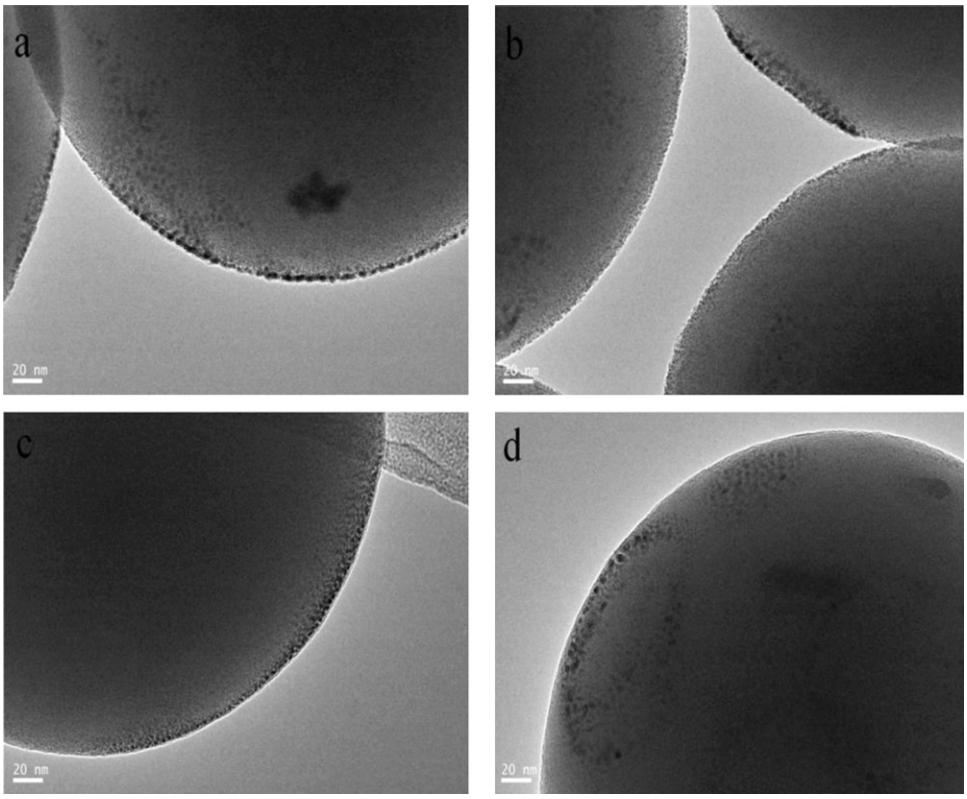

Fig. 1. The TEM micrographs of the catalysts: (a) Rh–Mn–Li/SiO_2, (b) Rh–Mn–Li–0.05Fe/SiO_2, (c) Rh–Mn–Li–0.1Fe/SiO_2 and (d) Rh–Mn–Li–0.5Fe/SiO_2.

Fig. 2 shows the TPR profiles for all the catalysts. It can be seen that the Rh–Mn–Li/SiO_2 catalyst exhibited three reduction peaks. According to the similar results reported previously, the high temperature peak centered at 300 °C is ascribed to the reduction of MnO_2 [15,20]. The peaks at 135 °C and 157 °C are ascribed to the reduction of Rh_2O_3 not intimately contacting with Mn species (denoted as Rh species I) and of Rh_2O_3 intimately contacting with Mn species (denoted as Rh species II), respectively [12,20]. The addition of Fe promoter changed the reducibility of Rh and Mn oxides, as shown in Fig. 2. More specifically, the reduction peaks of Rh oxides shifted to a higher temperature and the reduction peak of Mn oxides was moved to the lower temperature (190 °C) over Rh–Mn–Li–0.05%Fe/SiO_2 catalyst compared to that of Rh–Mn–Li/SiO_2 catalyst. This result suggests that the addition of 0.05 wt% Fe inhibited the reduction of Rh oxide species. Upon increasing the Fe loading, the two reduction peaks of Rh oxides gradually incorporated and shifted to lower temperatures, indicating that the reducibility of Rh oxide species over Rh–Mn–Li–Fe/SiO_2 catalyst was enhanced when the Fe loading was increased from 0.05 to 0.5 wt%. The result is in disagreement with the previous result reported in the literature [12], which showed that the TPR profile shapes remained unchanged when the amount of Fe was increased from 0.05 to 0.5 wt%.

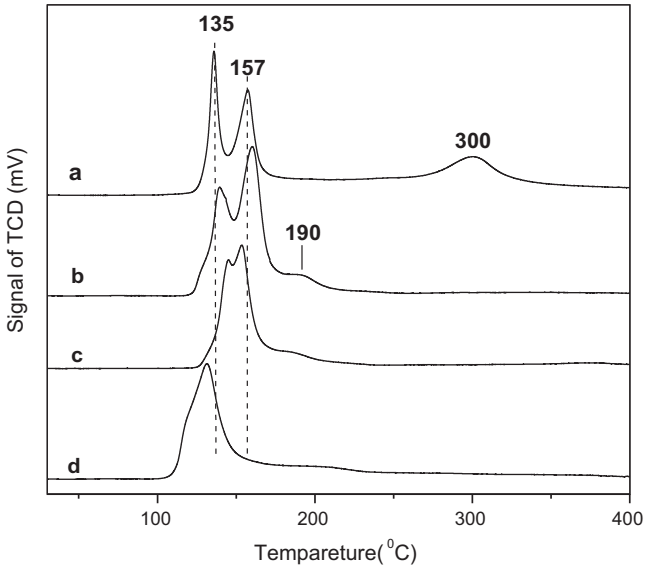

Fig. 2. The TPR profiles of Rh–Mn–Li/SiO_2 catalysts with different Fe loadings (a) 0%, (b) 0.05%, (c) 0.1%, (d) 0.5%.

Based on the TPR result, it is suggested that the Fe was in close contact with Rh and Mn, and the interaction between Rh and Mn gradually strengthened with the increase of Fe content. This process may affect the reduction of Rh and change the state of the active site, and thus influence the catalytic activity.

The desorption profiles of CO (m/z = 28) in Fig. 3 show that a similar associative desorption of CO took place on the catalysts, suggesting comparable strength of interaction of CO with respective catalyst surfaces. According to the research reported previously [21], the peaks at around 110 °C and 160 °C may be due to the desorption of weak adsorbed CO, such as the dicarbonyl $Rh^+(CO)_2$ [CO(gdc)] and linear adsorbed CO [CO(l)]. While, the last peak exceeded 250 °C may be assigned to the desorption of bridge bonded CO [CO(b)] or other forms which strongly adsorbed [21]. It is clear that the last peak shifted to higher temperature with the increase of Fe amount, suggesting that the addition of Fe could strengthen the strongly adsorbed CO. Moreover, it can be found from Fig. 3 and Table 1 that the total adsorbed CO decreased continuously with the Fe loading. This trend was also consistent with the results of CO uptake

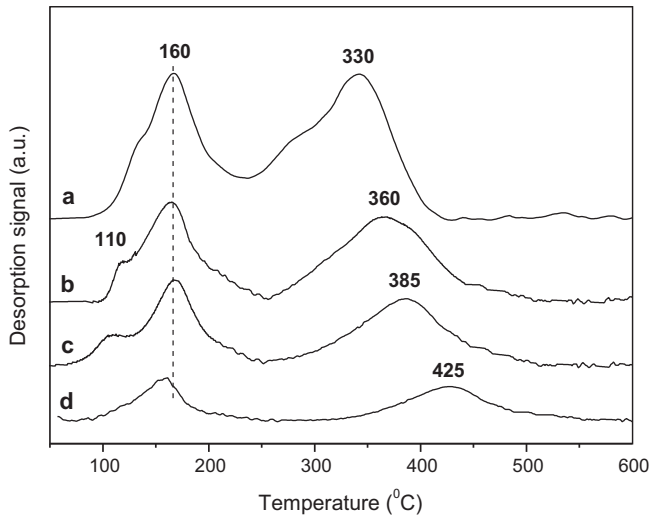

Fig. 3. The CO-TPD profiles of Rh–Mn–Li/SiO_2 catalysts with different Fe loadings (a) 0%, (b) 0.05%, (c) 0.1%, (d) 0.5%.

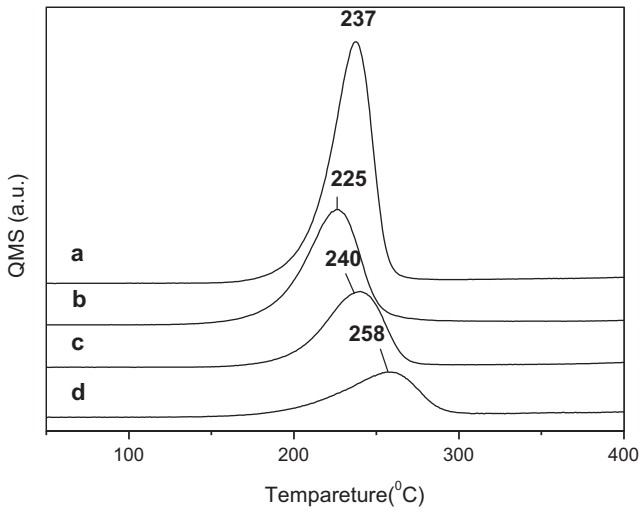

Fig. 5. The TPSR profiles of Rh–Mn–Li/SiO_2 catalysts with different Fe loadings (a) 0%, (b) 0.05%, (c) 0.1%, (d) 0.5%.

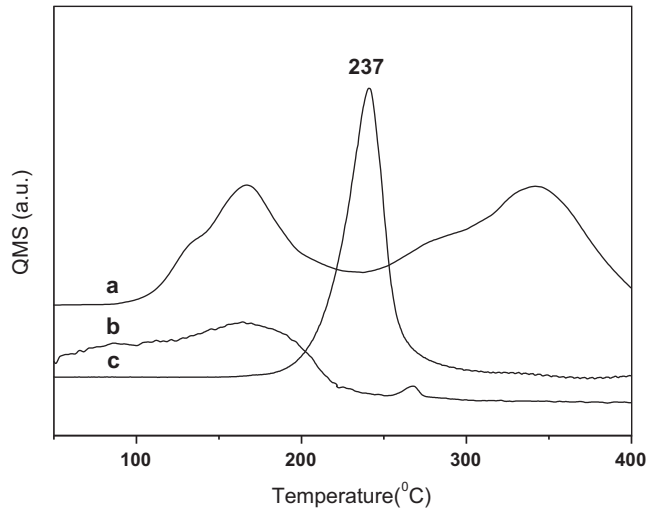

Fig. 4. Comparison of the desorption products for the TPD and TPSR of adsorbed CO on the Rh–Mn–Li/SiO_2. (a) CO desorption during CO-TPD, (b) CO desorption during TPSR, (c) CH_4 formation profile during TPSR.

observed by DRIFTS (see next); namely, redundant Fe would suppress the CO adsorption on the Rh surface. This result is inconsistent with that obtained by Yin et al. [12], who observed that when 0.05 wt% Fe was added to Rh–Mn–Li/SiO_2, the area of high temperature increased, but it decreased when the amount of Fe reached 0.5 wt%.

In order to understand how the adsorbed CO and H_2 might interact on the surface of Rh, TPSR experiments were carried out. Fig. 4 shows the CO-TPD and TPSR profiles on Rh–Mn–Li/SiO_2. It is obvious that only desorbed CO, which was attributed to the weakly adsorbed CO species on the Rh surface, was detected at temperatures lower than 250 °C in TPSR profile. Meanwhile, a sharp CH_4 peak centered at 237 °C appeared and the rate of methane formation dropped off sharply after the maximum, due to the depletion of adsorbed CO from the surface [12]. By combining the results of CO-TPD and TPSR, it is obvious that CH_4 is formed at the expense of the strongly adsorbed CO species and the weakly adsorbed CO desorbed easily, which is consistent with the conclusion drawn by Fujimoto et al. [22] and Rieck and Bell [23].

The TPSR experiments over Rh-based catalysts with different Fe loadings are shown in Fig. 5. It can be seen that the area of CH_4 peak decreased continuously with the Fe loading (see also Table 1), which was consistent with the result of CO-TPD. This result suggests a continuous decrease in the number of active sites for hydrogenation reaction [24,25], which may be ascribed to the deposition of Fe species on Rh [25]. On the other hand, when 0.05 wt% Fe was added to the Rh–Mn–Li/SiO_2 catalyst, the peak of CH_4 shifted from 237 to 225 °C. However, when the Fe loading was increased from 0.05 to 0.5 wt%, the peak of CH_4 shifted to lower temperatures over the Fe-containing catalysts. This result indicates that the ability of Rh to dissociate the CO molecules was increased by the addition of 0.05 wt% Fe, and then decreased with the increment of Fe loading, which can strongly affect the catalytic behavior, as will be noted later.

A series of infrared spectra of the in situ reduced catalysts with different Fe amounts after CO adsorption at 30 °C for 80 min followed by flushing with H_2/N_2 are compared in Fig. 6. It can be seen that the IR spectra of the adsorbed CO all exhibited a band at around 2067 cm^{-1} and a doublet at ~2104 and ~2035 cm^{-1} with different relative intensities after CO adsorption at 30 °C for 80 min as shown in Fig. 6 (time = 0 min). The 2067 cm^{-1} band can be attributed to the linear adsorbed CO [CO(l)] and the doublet can be assigned to the symmetric and asymmetric carbonyl stretching of the dicarbonyl $Rh^+(CO)_2$ [CO(gdc)] [26–28]. It is widely accepted that the CO(l) is formed on the Rh^0 sites, and CO(gdc) species is on the Rh^+ sites which may be highly dispersed [29,30]. As the

Table 1
Relative quantities of CO desorbed in CO-TPD experiments and CH_4 formed in TPSR experiments on catalysts and the corresponding CH_4/CO ratios.

Catalyst	Rh–Mn–Li/SiO_2	Rh–Mn–Li–0.05Fe/SiO_2	Rh–Mn–Li–0.1Fe/SiO_2	Rh–Mn–Li–0.5Fe/SiO_2
Amount of CO desorbed	1[a]	0.64	0.53	0.33
Amount of CH_4 formed	0.46	0.30	0.25	0.19
CH_4/CO	0.46	0.47	0.47	0.58

[a] The peak area of CO desorbed in CO-TPD over the Rh–Mn–Li/SiO_2 catalyst was quantitative for one unit; experimental error: ±5%.

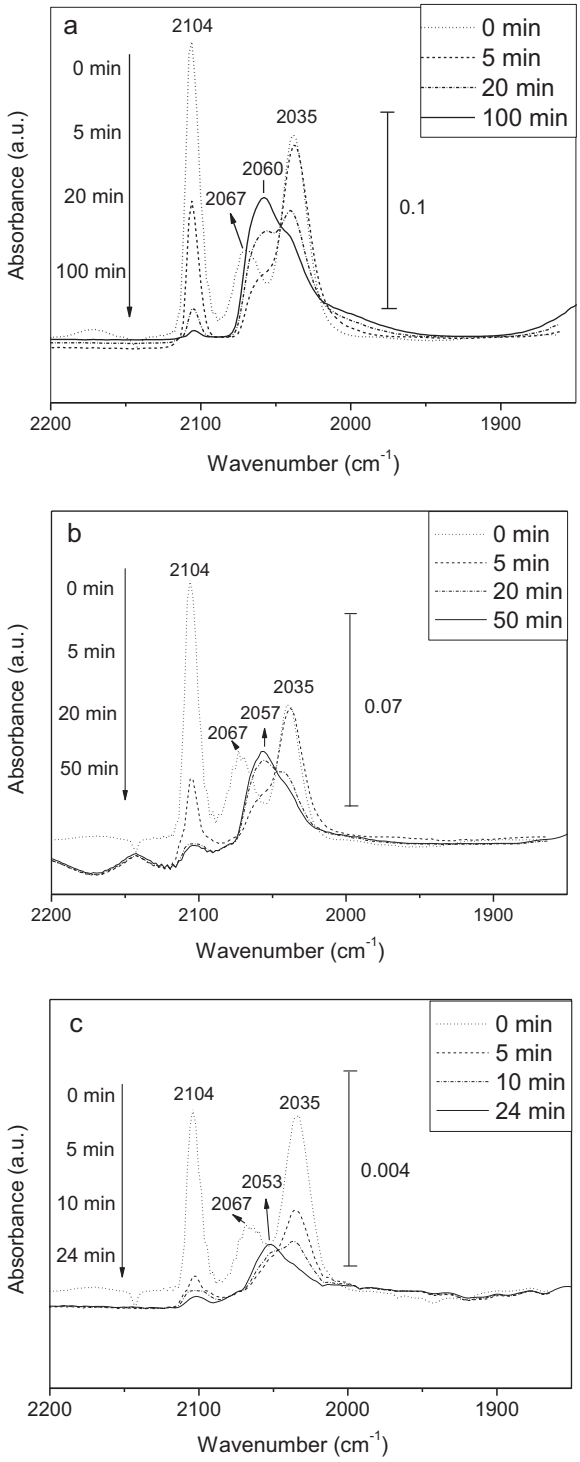

Fig. 6. The infrared spectra after CO adsorption at 30 °C for 80 min followed by flushing with H_2/N_2 (time = 0 min, start of H_2/N_2 flushing): (a) Rh–Mn–Li/SiO_2, (b) Rh–Mn–Li–0.05%Fe/SiO_2, (c) Rh–Mn–Li–0.1%Fe/SiO_2.

increase of Fe loading, the intensities of adsorbed CO decreased, and the decreasing rate of CO(l) was much faster than that of CO(gdc) as shown in Table 2.

Based on the above results, it can be inferred that Fe doping do not influence the highly dispersion of the metals due to the CO(gdc) species can only be formed on the Rh^+ sites that should be high dispersed. On the other hand, the addition of Fe can impede the CO adsorption, considering that the Rh coverage decreased due to the close contact between Fe and Rh, which is consistent with the result reported by Yin et al. [12]. By comparing the decreasing rate of CO(gdc) with that of CO(l), it is suggested that CO(gdc) is more stable on the Fe-promoted catalyst. Similarly, Haider et al. [3] have also reported that CO(gdc) which was the primary species on Rh/TiO_2 or Rh–Fe/TiO_2 at room temperature after exposure to CO was more thermally stable on the Fe-promoted catalyst.

Table 2
The ratios of peak areas of IR bands for the adsorbed CO species.[a]

Ratios	Catalyst		
	Rh–Mn–Li/SiO_2	Rh–Mn–Li–0.05Fe/SiO_2	Rh–Mn–Li–0.1Fe/SiO_2
CO(l)/CO(gdc)[b]	0.32	0.30	0.25
H–Rh–CO/CO(gdc)[c]	0.82	0.47	0.21

[a] The calculated data were based on the peak area of IR bands shown in Fig. 6; experimental error: ±5%.
[b] CO(l)/CO(gdc) denotes the peak area ratio of CO(l) versus CO(gdc) for the profile of Fig. 6 (time = 0 min).
[c] H–Rh–CO/CO(gdc) denotes the peak area ratio of the final H–Rh–CO species versus original CO(gdc) in Fig. 6.

For both the non and Fe promoted catalysts, the intensity of CO(l) decreased rapidly after the H_2/N_2 flushed. As the time increasing, the intensity of CO(gdc) decreased, along with the new bands at around 2055 cm^{-1} raised slowly. The 2055 cm^{-1} band can be attributed to rhodium carbonyl hydride species [H–Rh–CO] (i.e. re-formation of metallic Rh from isolated Rh^+) [30–32]. In related work, the researches by Guglielminotti et al. [11] and Solymosi and Pásztor [30] also gave IR spectra similar to our observation for the changes of CO adsorption in the presence of H_2, suggesting that the absorbed CO can be changed in the presence of H_2 at room temperature. By comparing the time required for the complete change of adsorbed CO over different catalysts, it can be inferred that the increased amount of Fe could promote the rate of transformation. Moreover, it can be seen from Table 2 that peak area ratios of the final H–Rh–CO species versus the original CO(gdc) on the catalysts decreased with the increase of Fe amount. This result suggests that the CO(gdc) species was changed simultaneously in two modes: (a) desorbed associatively; and (b) transformed into H–Rh–CO, and the addition of Fe could enhance the desorption mode rather than the transformation mode.

3.2. CO hydrogenation results

Firstly, the results of CO hydrogenation over the Rh–Mn–Li/SiO_2 catalyst at different reaction temperatures are presented in Table 3. As expected, CO conversion increased with the increase of reaction temperature. At the same time, the selectivity of products was also affected. For example, the methane selectivity increased at higher temperatures; however, the C_2^+ oxygenates selectivity decreased. It is important to note that the yield of C_2^+ oxygenates reached the maximum of 309.1 g/(kg h) at 300 °C.

Based on the above results, it can be found that the C_2^+ oxygenates yield is restricted by both the CO conversion and C_2^+ oxygenates selectivity. The CO conversion increased with the temperature, but the C_2^+ oxygenates selectivity decreased. Thus, the maximum of C_2^+ oxygenates yield appeared at 300 °C and dropped off sharply when the reaction temperature was further increased.

Typical time dependent changes of CO conversion and C_2^+ oxygenates selectivity over the representative Rh–Mn–Li–0.05Fe/SiO_2 catalyst are shown in Fig. 7. It can be seen that both the CO conversion and C_2^+ oxygenates selectivity decreased slowly during the first 14 h on stream, and were practically constant after 14 h on stream. Therefore, the data taken at 15–18 h on stream after steady state reached were used as indexes for reactivity of the catalysts.

Table 3
CO hydrogenation performance on the Rh–Mn–Li/SiO_2 catalyst at different temperatures.

Temperature (°C)	CO conv. (C%)	Selectivity of products (C%)							[c]STY (C_2^+ Oxy) (g/(kg h))
		CO_2	CH_4	MeOH	AcH	EtOH	C_2^+ Oxy[a]	C_2^+ HC[b]	
260	6.2	0.9	7.5	0	38.2	13.1	56.1	35.5	89.5
280	10.0	1.1	9.2	0	34.2	19.0	56.2	33.5	162.6
300	18.9	1.0	12.1	2.3	25.4	27.1	54.3	30.2	309.1
320	23.6	3.5	20.1	8.2	8.3	32.8	32.5	25.7	218.9

Reaction conditions: 3 MPa, SV = 10,000 mL/(g h), $V(H_2)/V(CO) = 2$, data taken after 15 h when steady state reached. Experimental error: ±5%.
[a] C_2^+ Oxy denotes oxygenates containing two and more carbon atoms.
[b] C_2^+ HC denotes hydrocarbons containing two and more carbon atoms.
[c] STY(C_2^+ Oxy): space time yield of C_2^+ Oxy.

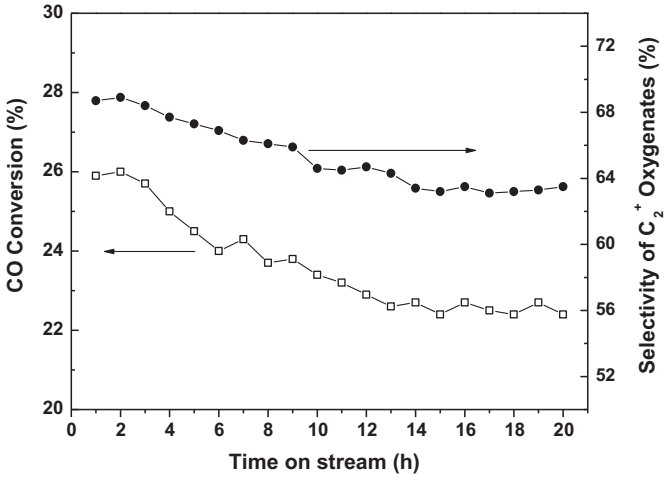

Fig. 7. CO conversion and C_2^+ oxygenates selectivity vs. time-on-stream for the Rh–Mn–Li–0.05Fe/SiO_2 catalyst (300 °C, 3.0 MPa, $V(H_2)/V(CO) = 2$, SV = 10,000 mL/(g h)): CO conversion (□) and C_2^+ oxygenates (●).

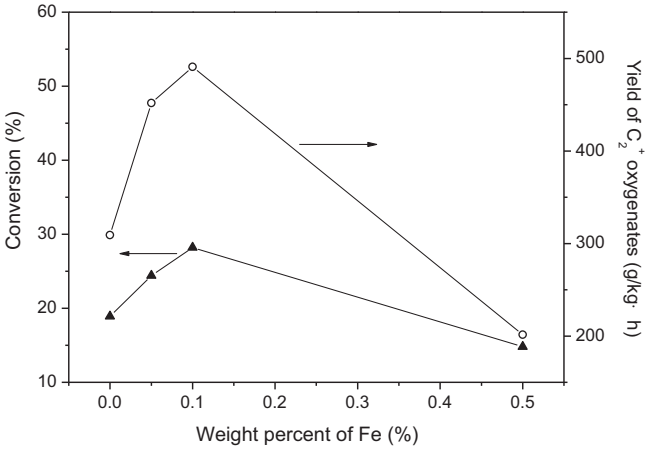

Fig. 8. Influence of the Fe loading on CO conversion and yield of C_2^+ oxygenates for CO hydrogenation over Fe-promoted Rh–Mn–Li/SiO_2 (300 °C, 3.0 MPa, $V(H_2)/V(CO) = 2$, SV = 10,000 mL/(g h)).

As shown in Figs. 8 and 9, the addition of different amounts of Fe promoter modified the catalytic properties of the Rh–Mn–Li/SiO_2 catalyst. As observed in Fig. 8, the C_2^+ oxygenates yield had the maximum of 491.0 g/(kg h) when the Fe content was 0.1 wt% due to the CO conversion increased firstly and then decreased rapidly when the amount of Fe exceeded 0.1 wt%.

In principle, it is conceivable that the increased amount of promoter could partially block the Rh surface, thereby diminishing the number of active sites, which was consistent with the results of DRIFTS and CO-TPD. On the other hand, our IR experiment also found that the addition of Fe increased the desorption/transformation rate of CO(gdc), resulting in an increase in the rate of CO conversion; that is, the increment in the CO conversion would be due to a higher catalytic activity per Rh site. Combing the above two opposing effects, the CO conversion appeared the maximum when the Fe content reached 0.1 wt%. Results reported by Yin et al. [12] and Chen et al. [25] are similar to the above observation, although the highest CO conversion and yield of C_2^+ oxygenates reached at the different Fe amount due to the different experimental conditions used (Rh loading, temperature, space velocity, etc.).

Doping of Fe also plays a crucial role in promoting the selectivity toward main products. As shown in Fig. 9, the selectivity of CH_4 did not change noticeably when lower amount of Fe (≤0.1 wt%) was added to the Rh–Mn–Li/SiO_2 catalyst, but it increased sharply when the Fe loading was increased from 0.1 to 0.5 wt%. By combining the results of CO-TPD with TPSR, it is obvious that CH_4 is formed at the expense of the strongly adsorbed CO species, and the relative ratios of CH_4 formation versus CO desorption were unchanged when doping lower amount of Fe (≤0.1 wt%) and increased significantly with the addition of 0.5 wt% Fe (Table 1). This can reasonably explain the change of CH_4 selectivity over the Rh–Mn–Li/SiO_2 catalysts doped with different amounts of Fe.

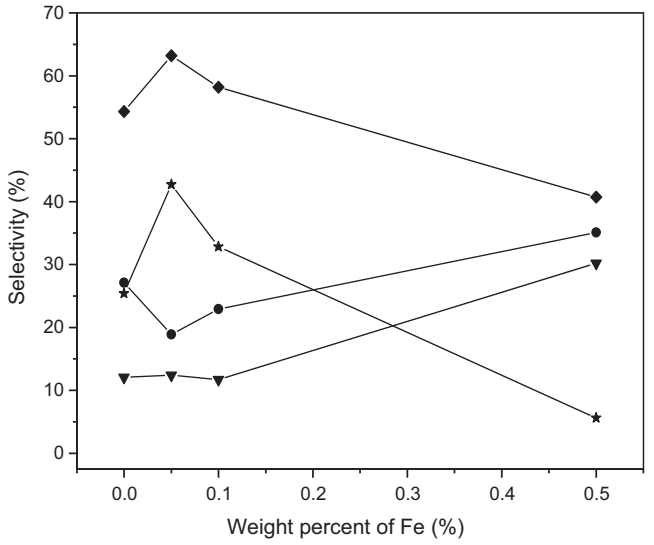

Fig. 9. Influence of the Fe loading on the CO hydrogenation selectivity over Fe-promoted Rh–Mn–Li/SiO_2 (300 °C, 3.0 MPa, $V(H_2)/V(CO) = 2$, SV = 10,000 mL/(g h)): methane (▼), ethanol (●), acetaldehyde (★), C_2^+ oxygenates (◆).

Regarding the formation of oxygenates, the selectivity of C_2^+ oxygenates had a maximum when the Fe content was 0.05 wt%, then decreased with the further addition of Fe (Fig. 9). This result was at variance with that obtained by Yin et al. [12], who reported that the selectivity of C_2^+ oxygenates did not change when the Fe content was increased from 0 to 0.05 wt%. Furthermore, the selectivity of ethanol decreased when 0.05 wt% Fe was added into Rh–Mn–Li/SiO_2 catalyst. However, with the further increase of Fe content, the selectivity of ethanol increased notably, along with the decrease of acetaldehyde selectivity.

It is well acknowledged that Rh^0 is the active center for CO dissociation, and Rh^+ sites are responsible for CO insertion to form intermediates of C_2 oxygenates [33–35]. Moreover, it was reported that the cationic Rh sites was more active for CO insertion, leading to higher C_2 oxygenates selectivity than reduced Rh sites [36]. In the present work, the TPR result (Fig. 2) indicated that the reducibility of Rh oxide species over the Rh–Mn–Li/SiO_2 catalyst was decreased upon the addition of 0.05 wt% Fe, but then increased with more content of Fe. The order of reducibility is exactly in reverse order of selectivity to C_2^+ oxygenates (Fig. 9). This result is well consistent with the observation by Schwartz et al. [37], who reported that over Rh–Li–Mn/TiO_2 catalyst the selectivity to C_2^+ oxygenates varies inversely with the reducibility of Rh metal, that is, the lower the reducibility of Rh, the higher the selectivity to C_2^+ oxygenates. Furthermore, by comparing the decrease of C_2^+ oxygenates selectivity with the decreased ratios of the finally transform of H–Rh–CO versus the original CO(gdc), it can be inferred that the depressed transformation of CO(gdc) into H–Rh–CO caused by the addition of Fe might be not conducive to the formation of C_2 oxygenates [38]. In fact, many researchers have previously proposed that the H–Rh–CO species formed from CO(gdc) species during CO hydrogenation, could be the intermediate for the formation of C_2 oxygenates [8,29,30]. On the other hand, the decreased ratio of acetaldehyde/ethanol (AcH/EtOH) with the increased Fe amount suggested that Fe enhances hydrogenation ability and boosts the hydrogenation of AcH to EtOH, which is consistent with the conclusion drawn by Burch and Petch [17].

4. Conclusions

The effects of the loading of Fe promoter on the activity and selectivity of Rh–Mn–Li/SiO_2 catalyst for the synthesis of C_2^+ oxygenates from syngas were explored. The results showed that the promoter of Fe greatly affected the catalytic performance of Rh–Mn–Li/SiO_2 on CO hydrogenation: Fe could improve the CO conversion and increase the yield of C_2^+ oxygenates when the loading amount was very low ($\leq$0.1 wt%); but high adding amount of Fe (>0.1 wt%) would reverse this effect.

The H_2-TPR result showed that the Fe was in close contact with Rh and Mn, and the interaction between Rh and Mn gradually strengthened with the increase of Fe content. On the other hand, the addition of different amounts of Fe affected differently the reducibility of Rh oxide species. Based on the result of CO-TPD and TPSR, it is further proved that CO uptake decreased with the increased quantity of Fe addition, and only the strongly adsorbed CO could be hydrogenated to CH_4, while the addition of Fe could strengthen the strongly adsorbed CO. Based on the IR results and the catalytic performance of the catalysts for CO hydrogenation, it is conceivable that the catalytic activity is restricted by both the total CO adsorption capacity and the desorption/transform rate of adsorbed CO: when the desorption/transformation rate of CO(gdc) dominates at the low values of Fe loading ($\leq$0.1 wt%), the increment of desorption/transformation rate is favorable to the increase of CO conversion; however, at the high values of Fe loading (>0.1 wt%), the CO conversion will decrease due to the decreasing CO adsorption caused by decreased Rh coverage. On the other hand, Fe enhances hydrogenation ability and boosts the hydrogenation of AcH to EtOH. The selectivity to C_2^+ oxygenates varied inversely with the reducibility of Rh oxide species. Moreover, H–Rh–CO species formed from CO(gdc) species might be the intermediate for the formation of C_2^+ oxygenates, and the addition of Fe could depress the transformation of CO(gdc) into H–Rh–CO, which might inhibit the formation of C_2^+ oxygenates.

Acknowledgements

The authors gratefully acknowledge financial support from the Science and Technology Commission of Shanghai Municipality (08520513600), Leading Academic Discipline Project of Shanghai Education Committee (J51503) and Shanghai Special Fund for Outstanding Young Teachers (yyy10083). The helpful suggestions and linguistic revision of the manuscript provided by the anonymous reviewers are also gratefully acknowledged.

References

[1] G. Mayank, L.S. Miranda, J.S. James, ACS Catalysis 1 (2011) 641.
[2] R.S. Venkateswara, K.D. Ajay, K. Janusz, Applied Catalysis A: General 404 (2011) 1.
[3] M.A. Haider, M.R. Gogate, R.J. Davis, Journal of Catalysis 261 (2009) 9.
[4] S.S.C. Chuang, R.W. Stevens Jr., R. Khatri, Topics in Catalysis 32 (2005) 225.
[5] J.P. Hindermann, G.J. Hutchings, A. Kiennemann, Catalysis Reviews: Science and Engineering 35 (1993) 1.
[6] S. Ho, Y. Su, Journal of Catalysis 168 (1997) 51.
[7] D.H. Jiang, Y.J. Ding, Z.D. Pan, W.M. Chen, H.Y. Luo, Catalysis Letters 121 (2008) 241.
[8] F. Solymosi, I. Tombacz, M. Kocsis, Journal of Catalysis 75 (1982) 78.
[9] P. Basu, D. Panayotov, J.T. Yates Jr., Journal of the American Chemical Society 110 (1988) 2074.
[10] J.J. Spivey, A. Egbebi, Chemical Society Reviews 36 (2007) 1514.
[11] E. Guglielminotti, F. Pinna, M. Rigoni, G. Strukul, L. Zanderighi, Journal of Molecular Catalysis A: Chemical 103 (1995) 105.
[12] H.M. Yin, Y.J. Ding, H.Y. Luo, H.J. Zhu, D.P. He, J.M. Xiong, L.W. Lin, Applied Catalysis A: General 243 (2003) 155.
[13] H.Y. Luo, P.Z. Lin, S.B. Xie, H.W. Zhou, C.H. Xu, S.Y. Huang, L.W. Lin, D.B. Liang, P.L. Yin, Q. Xin, Journal of Molecular Catalysis A: Chemical 122 (1997) 115.
[14] H. Arakawa, T. Fukushima, M. Ichikawa, S. Natsushita, K. Takeuchi, T. Matsuzaki, Y. Sugi, Chemistry Letters 14 (1985) 881.
[15] X. Mo, J. Gao, N. Umnajkaseam, J.G. Goodwin Jr., Journal of Catalysis 267 (2009) 167.
[16] J. Yu, D.S. Mao, L.P. Han, Q.S. Guo, G.Z. Lu, Catalysis Communications 24 (2012) 25.
[17] R. Burch, M.I. Petch, Applied Catalysis A: General 88 (1992) 39.
[18] J.J. Wang, Q.H. Zhang, Y. Wang, Catalysis Today 171 (2009) 257.
[19] R. Burch, M.I. Petch, Applied Catalysis A: General 88 (1992) 77.
[20] D.H. Jiang, Y.J. Ding, Z.D. Pan, X.M. Li, G.P. Jiao, J.W. Li, W.M. Chen, H.Y. Luo, Applied Catalysis A: General 331 (2007) 70.
[21] Y. Wang, H.Y. Luo, D.B. Liang, X.H. Bao, Journal of Catalysis 196 (2000) 46.
[22] K. Fujimoto, M. Kameyama, J. Kunugi, Journal of Catalysis 61 (1980) 7.
[23] J.S. Rieck, A.T. Bell, Journal of Catalysis 96 (1985) 88.
[24] M. Ojeda, M.L. Granados, S. Rojas, P. Terreros, F.J. García-García, J.L.G. Fierro, Applied Catalysis A: General 261 (2004) 47.
[25] G.C. Chen, C.Y. Guo, Z.J. Huang, G.Q. Yuan, Chemical Engineering Research and Design 89 (2011) 249.
[26] A.C. Yang, C.W. Garland, Journal of Physical Chemistry 61 (1957) 1504.
[27] F. Solymosi, M. Pasztor, Journal of Physical Chemistry 89 (1985) 4789.
[28] J. Gao, X. Mo, A.C. Chien, W. Torres, J.G. Goodwin Jr., Journal of Catalysis 262 (2009) 119.
[29] P. Basu, D. Panayotov, J.T. Yates, Journal of Physical Chemistry 91 (1987) 3133.
[30] F. Solymosi, M. Pásztor, Journal of Physical Chemistry 90 (1986) 5312.
[31] F. Solymosi, A. Erdöhelyi, M. Kocsis, Journal of Catalysis 65 (1980) 428.
[32] M.L. McKee, C.H. Dai, S.D. Worley, Journal of Physical Chemistry 92 (1988) 1056.
[33] P.R. Watson, G.A. Somorjai, Journal of Catalysis 72 (1981) 347.
[34] M. Kawai, M. Uda, M. Ichikawa, Journal of Physical Chemistry 89 (1985) 1654.
[35] L.P. Han, D.S. Mao, J. Yu, Q.S. Guo, G.Z. Lu, Catalysis Communications 23 (2012) 20.
[36] S.S.C. Chuang, S.I. Pien, Journal of Catalysis 135 (1992) 618.
[37] V. Schwartz, A. Campos, A. Egbebi, J.J. Spivey, S.H. Overbury, ACS Catalysis 1 (2011) 1298.
[38] J. Yu, D.S. Mao, L.P. Han, Q.S. Guo, G.Z. Lu, Catalysis Communications 27 (2012) 1.